The Journal of Immunology

DCIR Maintains Bone Homeostasis by Regulating IFN- γ Production in T Cells

Takumi Maruhashi, Tomonori Kaifu, Rikio Yabe, Akimasa Seno, Soo-Hyun Chung, Noriyuki Fujikado and Yoichiro Iwakura

J Immunol 2015; 194:5681-5691; Prepublished online 29 April 2015;
doi: 10.4049/jimmunol.1500273
http://www.jimmunol.org/content/194/12/5681

The Journal of Immunology is published twice each month by
The American Association of Immunologists, Inc.,
1451 Rockville Pike, Suite 650, Rockville, MD 20852

Print ISSN: 0022-1767 Online ISSN: 1550-6606.

DCIR Maintains Bone Homeostasis by Regulating IFN-γ Production in T Cells

Takumi Maruhashi,[*,†,‡,1,2] Tomonori Kaifu,[*,‡,§,1] Rikio Yabe,[*,‡,¶] Akimasa Seno,[*,¶] Soo-Hyun Chung,[*,‡] Noriyuki Fujikado,[*,§,3] and Yoichiro Iwakura[*,†,‡,§,¶]

Dendritic cell immunoreceptor (DCIR) is a C-type lectin receptor mainly expressed in DCs. *Dcir*$^{-/-}$ mice spontaneously develop autoimmune enthesitis and ankylosis accompanied by fibrocartilage proliferation and ectopic ossification. However, the mechanisms of new bone/cartilage formation in *Dcir*$^{-/-}$ mice remain to be elucidated. In this study, we show that DCIR maintains bone homeostasis by regulating IFN-γ production under pathophysiological conditions. DCIR deficiency increased bone volume in femurs and caused aberrant ossification in joints, whereas these symptoms were abolished in *Rag2*$^{-/-}$*Dcir*$^{-/-}$ mice. IFN-γ–producing T cells accumulated in lymph nodes and joints of *Dcir*$^{-/-}$ mice, and purified *Dcir*$^{-/-}$ DCs enhanced IFN-γ^{+} T cell differentiation. The ankylotic changes and bone volume increase were suppressed in the absence of IFN-γ. Thus, IFN-γ is a positive chondrogenic and osteoblastogenic factor, and DCIR is a crucial regulator of bone metabolism; consequently, both factors are potential targets for therapies directed against bone metabolic diseases. *The Journal of Immunology*, **2015, 194: 5681–5691.**

The C-type lectin receptors (CLRs) are a group of transmembrane proteins with one or more extracellular carbohydrate recognition domains that bind their ligands in a calcium-dependent manner (1). CLRs are generally regarded as pattern recognition receptors that sense conserved molecular patterns on bacterial and fungal cell surfaces and initiate innate and adaptive immune responses against pathogens (1). Dendritic cell immunoreceptor (DCIR, *Clec4a2*), a CLR family member, is predominantly expressed in DCs and macrophages (2, 3). DCIR has an ITIM in the cytoplasmic region (4, 5) and negatively controls multiple signaling pathways in hematopoietic cells (4) by recruiting the SH2 domain–containing protein tyrosine phosphatases (SHP)-1 and SHP-2 (5, 6). Previously, we showed that aged *Dcir*-deficient (*Dcir*$^{-/-}$) mice spontaneously develop autoimmune sialadenitis and enthesitis, an inflammation at sites of attachment of ligaments, tendons, and joint capsules to bones (3). Moreover, *Dcir*$^{-/-}$ mice are highly susceptible to collagen-induced arthritis. This is because DCIR negatively regulates differentiation and proliferation of DCs by suppressing GM-CSF signaling (3). The DC population is excessively expanded in *Dcir*$^{-/-}$ mice, causing development of autoimmunity and high susceptibility to Ag stimulation (3). DCIR is also implicated in the downregulation of TLR8- and TLR9-mediated cytokine production (7, 8). Thus, DCIR is critically important for the homeostasis of the immune system. Furthermore, we showed that ankylotic changes occur in joints of *Dcir*$^{-/-}$ mice, accompanied by fibrocartilage proliferation and heterotopic ossification (3). However, the pathogenic mechanism by which DCIR deficiency induces these bone abnormalities remains elusive.

Bone tissue is constantly reconstructed by a dynamic balance between bone-forming osteoblasts and bone-resorbing osteoclasts (9). The functions of osteoclasts and osteoblasts are coordinately controlled bidirectionally between osteoblasts and osteoclasts by mediators such as growth factors, cytokines, hormones, and matrix proteins (10). Two cytokines play crucial roles in osteoclastogenesis: M-CSF and receptor activator of NF-κB ligand (RANKL); these factors are produced by osteoblasts, osteocytes, and bone marrow stromal cells (10–12). Alternatively, osteoclasts release several factors that control osteoblast motility into sites of bone resorption and activate bone formation (10, 13–15). Therefore, the imbalance between bone destruction and regeneration results in skeletal diseases such as osteoporosis and osteopetrosis (16). Furthermore, a number of proinflammatory cytokines produced by T cells, such as IFN-γ, inhibit osteoclastogenesis by acting on osteoclast precursor cells (17, 18). In contrast, TNF and IL-1 stimulate osteoclastogenesis by inducing RANKL expression in osteoblasts and stromal cells, as well as by directly stimulating

*Center for Experimental Medicine and Systems Biology, Institute of Medical Science, The University of Tokyo, Tokyo 108-8639, Japan; †Department of Biophysics and Biochemistry, Graduate School of Science, The University of Tokyo, Tokyo 113-0032, Japan; ‡Research Institute for Biomedical Sciences, Tokyo University of Science, Chiba 278-0022, Japan; §Core Research for Evolutional Science and Technology, Japan Science and Technology Agency, Saitama 332-0012, Japan; and ¶Medical Mycology Research Center, Chiba University, Chiba 250-8673, Japan

[1]T.M. and T.K. contributed equally to this work.

[2]Current address: Division of Immune Regulation, Institute for Genome Research, Tokushima University, Tokushima, Japan.

[3]Current address: Division of Immunology, Harvard Medical School, Boston, MA.

Received for publication February 4, 2015. Accepted for publication April 3, 2015.

This work was supported by Grant-in-Aid for Scientific Research (S) 24220011 (to Y.I.) and Grant-in-Aid for Scientific Research (C) 23500489 (to T.K.) from the Japan Society for the Promotion of Science; a Core Research for Evolutional Science and Technology Grant from the Japan Science and Technology Agency (to Y.I.); the Science and Technology Research Promotion Program for Agriculture, Forestry, Fisheries, and Food Industry (to Y.I.); and by a fellowship from the Japan Society for the Promotion of Science (to T.M.).

T.M. and T.K. designed, performed, and analyzed most of the experiments; R.Y., A.S., S.-H.C., and N.F. helped perform experiments and analyzed data; T.M. and T.K. wrote the manuscript; and Y.I. organized and supervised the project and edited the draft manuscript.

Address correspondence and reprint requests to Prof. Yoichiro Iwakura, Research Institute for Biomedical Sciences, Tokyo University of Science, 2669 Yamazaki, Noda, Chiba 278-0022, Japan. E-mail address: iwakura@rs.tus.ac.jp

The online version of this article contains supplemental material.

Abbreviations used in this article: AS, ankylosing spondylitis; CLR, C-type lectin receptor; COL2, type II collagen; μCT, micro–computed tomography; 3D, three-dimensional; DC, dendritic cell; DCIR, dendritic cell immunoreceptor; GMA, glycol methacrylate; LN, lymph node; MMP3, matrix metalloproteinase-3; PCNA, proliferating cell nuclear Ag; RANKL, receptor activator of NF-κB ligand; SHP, Src homology region 2 domain–containing phosphatase; SOX9, sex-determining region Y–box 9; WT, wild-type.

RANKL signaling in osteoclast precursors (19, 20). Th17 cells and IL-17, which induces RANKL expression on osteoblasts and fibroblasts, stimulate osteoclastogenesis, causing bone erosion (17). Therefore, bone metabolism is greatly influenced by the immune system.

Ankylosing spondylitis (AS), a form of seronegative spondyloarthritis, is characterized by axial and peripheral enthesitis, followed by joint immobility due to heterotopic cartilage and bone formation (21, 22). Intensive clinical investigations and genome-wide association studies suggest the involvement of HLA-B27, a class I MHC allele, and proinflammatory cytokines such as TNF and IL-23 in the pathogenesis of AS (23–27). Ankylotic changes of joints are also associated with the bone-remodeling mediators such as bone morphogenetic proteins, wingless proteins, and their endogenous inhibitor dickkopf-1 (28, 29). The expression of these mediators in synovial cells and stromal cells is also regulated by inflammatory cytokines, such as TNF, IL-17, and IL-1 (28, 30–32), suggesting the involvement of these cytokines in the development of ankylotic changes. However, the precise mechanisms underlying the aberrant cartilage and bone formation seen in AS still remain to be elucidated.

In this study, we analyzed the pathogenic mechanisms of ankylosis in *Dcir*$^{-/-}$ mice. We showed that articular changes were completely suppressed in RAG2-deficient (*Rag2*$^{-/-}$) mice, indicating an immune-mediated pathology. Furthermore, joint ankylosis was completely abolished in *Tnf*$^{-/-}$*Dcir*$^{-/-}$ and *Ifng*$^{-/-}$*Dcir*$^{-/-}$ mice, but not in *Il17a*$^{-/-}$*Dcir*$^{-/-}$ mice, suggesting that TNF and IFN-γ are crucial for the development of ankylosis in *Dcir*$^{-/-}$ mice. Furthermore, a mild increase of bone volume was observed in *Dcir*$^{-/-}$ mice, and this was also normalized in *Rag2*$^{-/-}$ and *Ifng*$^{-/-}$ mice. We showed that IFN-γ–producing T cells are effectively induced in *Dcir*$^{-/-}$ mice, and IFN-γ has potent chondrogenic and osteogenic activity. These observations suggest that DCIR is a possible target for the treatment of bone metabolic diseases.

Materials and Methods

Mice

Dcir (*Clec4a2*)$^{-/-}$ mice (3), *Ifng*$^{-/-}$ mice (33), and *Il17a*$^{-/-}$ mice (34) were generated as described and backcrossed to C57BL/6J mice (Japan SLC, Shizuoka, Japan) for 9–12 generations before they were used in this study. *Tnf*$^{-/-}$ mice (35) were backcrossed to C57BL/6J mice for 12 generations. C57BL/6J *Rag2*$^{-/-}$ mice were obtained from the Central Institute for Experimental Animals (Kawasaki, Japan). *Rag2*$^{-/-}$*Dcir*$^{-/-}$, *Ifng*$^{-/-}$*Dcir*$^{-/-}$, *Il17a*$^{-/-}$*Dcir*$^{-/-}$, and *Tnf*$^{-/-}$*Dcir*$^{-/-}$ mice were generated by intercrossing *Rag2*$^{-/-}$, *Ifng*$^{-/-}$, *Il17a*$^{-/-}$, and *Tnf*$^{-/-}$ mice with *Dcir*$^{-/-}$ mice, respectively. C57BL/6J wild-type (WT) mice were purchased from Japan SLC. Male mice of similar ages were used for experiments. These mice were housed under specific pathogen–free conditions in environmentally controlled clean rooms at the Institute of Medical Science (University of Tokyo) and the Research Institute for Biomedical Sciences (Tokyo University of Science). All animal experiments were approved by the animal use committees of both universities and were conducted according to the institutional ethics guidelines for animal experiments and safety guidelines for gene manipulation experiments.

Histology and micro–computed tomography analysis

Ankle joints were fixed with neutralized 10% formalin overnight at 4°C, decalcified with 10% EDTA (Nacalai Tesque, Kyoto, Japan) in PBS (pH 7.4) for 2–3 wk, embedded in paraffin, sectioned (5 μm), and stained with H&E or Safranin O/Fast Green (Waldeck, Münster, Germany). For micro–computed tomography (μCT), ankle joints and femurs were fixed and analyzed using an R_μXT (Rigaku, Tokyo, Japan) or a Scan Xmate-L090 (Comscantecno, Yokohama, Japan). Three-dimensional image analyses were performed using the TRI/3D-BON software (Ratoc System Engineering, Tokyo, Japan). Trabecular bone mineral density was characterized by calculating bone volume density (bone volume/tissue volume), trabecular thickness (2 × bone volume/bone surface), trabecular number [(bone volume/tissue volume)/trabecular thickness], and trabecular separation [1/(trabecular number − trabecular thickness)]. The trabecular number was defined as the number of trabecular bones.

Quantitative real-time RT-PCR analysis

Total mRNA was extracted from joint-infiltrating cells, chondrocytes, and osteoblasts using the GenElute mammalian RNA miniprep kit (Sigma-Aldrich, St. Louis, MO). Isolated RNA was then subjected to reverse transcription using a high-capacity cDNA reverse transcription kit (Applied Biosystems, Foster City, CA). Gene expression was analyzed by quantitative PCR using SYBR premix Ex Taq (Takara Bio, Otsu, Japan) on an iCycler (Bio-Rad, Hercules, CA). Specific primer sets are described in Supplemental Table I. Data were normalized to *Gapdh* or *Actb*.

Calcein labeling

Dynamic histomorphometric analysis of bone formation was carried out by Kureha Special Laboratory (Fukushima, Japan). Body weights of WT and *Dcir*$^{-/-}$ mice at 8 wk of age were measured, and the mice were i.p. administered 16 mg/kg (body weight) of calcein (Nacalai Tesque) twice at 2-d intervals. The mice were sacrificed on day 2 after the last injection of calcein. Tibiae were cleaned of soft tissue and muscle, and then fixed in 70% ethanol for 1 wk with the ethanol replaced every day. The mineralization regions were stained as green lines. The undecalcified bone tissues were placed in methyl benzoate for 15 min to facilitate the infiltration of glycol methacrylate (GMA) into the tissues, and then immersed in 5% methyl benzoate in GMA at 4°C, which was replaced three times during a period of 2 h. Then, these bone tissues were embedded in GMA. We prepared 3-μm sections of tibiae using a microtome (Sakura Finetek Japan, Tokyo, Japan) and detected incorporated fluorescence at the mineralization front. For studies of dynamic bone formation, the mineralizing surface (mineralization surface/bone surface; %), mineral apposition rate (μm/d), and bone formation rate (bone formation rate/bone surface; $\mu m^3/\mu m^2$/d) were determined at ×400 magnification using an image analyzer (System Supply, Nagano, Japan).

Bone histomorphometric analysis

A histomorphometric analysis of murine tibiae was performed by Kureha Special Laboratory. The bones of WT and *Dcir*$^{-/-}$ mice were isolated from five to six 8-wk-old mice per group and fixed with 70% ethanol. To measure the histomorphometric parameters of the bone structure, 3-μm sections of GMA-embedded femur tissues were stained with toluidine blue. The trabecular bone parameter was determined in an area of the secondary spongiosa with a 1.05 mm width at 0.3 mm from the growth plate. The trabecular bones in metaphysis were examined with a HistometryRT camera. For assays of osteoclast number (osteoclast number/100 mm) and osteoclast surface (osteoclast surface/bone surface; %), osteoclasts were defined as cells with more than one nucleus that formed resorption lacunae at the surface of the trabeculae. Parameters of bone remodeling, including the osteoblast number (osteoblast number/100 mm) and osteoblast surface (osteoclast surface/bone surface; %), were measured in toluidine blue–stained sections.

Cell preparation and flow cytometry

For joint-infiltrating cell preparations, the ankle joints, after removal of skin and bone marrow, were digested with 5 mg/ml collagenase type II (Worthington Biochemical, Lakewood, NJ) in RPMI 1640 (Life Technologies/Invitrogen, Carlsbad, CA) with 5% FCS (Life Technologies) at 37°C for 90 min. For coculture with T cells and DCs, T cells were purified from spleens of WT mice using an autoMACS Pro separator with CD90.2 MicroBeads (Miltenyi Biotec, Bergisch Gladbach, Germany). CD11c^{hi} DCs were sorted using a FACSAria II (BD Biosciences, Franklin Lakes, NJ) from the spleens of WT and *Dcir*$^{-/-}$ mice after removal of CD90.2$^+$ and B220$^+$ cells by magnetic cell sorting, and 2 × 10^4 cells were cocultured with 2 × 10^5 CD90.2$^+$ T cells for 3 d in the presence of 1 μg/ml soluble anti-CD3 Ab (145-2C11, eBioscience, San Diego, CA). Fluorescence-conjugated Abs to CD3 (clone 145-2C11), CD4 (RM4-5), CD8 (53-6.7), IFN-γ (XMG1.2), IL-17 (TC11-18H10), CD45 (30-F11), CD11c (N418), CD11b (M1/70), CD80 (16-10A1), CD86 (GL-1), CD40 (3/23), and I-A/I-E (M5/114.15.2) were obtained from BioLegend (San Diego, CA) or eBioscience. For intracellular cytokine staining, cells were incubated with PMA (50 ng/ml, Sigma-Aldrich), ionomycin (500 ng/ml, Sigma-Aldrich), and monensin (2 μM, Sigma-Aldrich) for 5 h. After surface staining, cells were fixed and permeabilized using an intracellular fixation and permeabilization buffer set (eBioscience) and then stained for intracellular cytokines. Data were acquired on a FACSCanto II (BD Biosciences) and analyzed using the FlowJo software (Tree Star, Ashland, OR).

Measurement of IFN-γ–producing T cells in peripheral blood

Whole blood was obtained from mice under anesthesia by cardiac puncture with a 21-gauge needle attached to a syringe containing heparin (Mochida Pharmaceutical, Tokyo, Japan). The blood samples were mixed with 10 volumes of hemolysis buffer and left on ice for 10 min, followed by centrifugation at 1500 rpm at 4˚C for 5 min to collect mononuclear cells. The hemolysis buffer treatment was repeated three times. PBMCs underwent stimulation for 5 h with PMA (50 ng/ml), ionomycin (500 ng/ml), and brefeldin A (10 μg/ml) during the entire incubation period. IFN-γ secretion by PBMCs was detected by intracellular molecular staining and flow cytometric analysis.

Joint protein extraction

Ankle joints, after removal of skin and bone marrow, were homogenized in liquid nitrogen, and proteins were extracted with a lysis buffer containing 50 mM Tris-HCl (pH 7.5), 100 mM NaCl, and 0.1% Triton X-100.

Serum collection

Whole blood was obtained by cardiac puncture under anesthesia. The blood samples were left to clot at 4˚C overnight and then centrifuged at 3000 rpm for 10 min to separate serum from coagulated blood. The serum was collected and stored at −80˚C prior to assays.

ELISA

IFN-γ, IL-17A, and TNF were measured using the mouse IFN-γ DuoSet (R&D Systems, Minneapolis, MN), the mouse IL-17A ELISA Ready-SET Go! kit (eBioscience), and the mouse TNF-α ELISA MAX standard (BioLegend). The serum levels of IFN-γ were determined using the IFN-γ ELISA kit (Mabtech, Nacka Strand, Sweden). Absorbance was measured on an MTP-300 microplate reader (Hitachi, Tokyo, Japan).

Murine chondrocyte primary culture

Primary cultures of murine chondrocytes were performed according to Gosset et al. (36). Murine chondrocytes were prepared from costal cartilage tissue of newborn mice (5–6 d) by enzymatic digestion in DMEM (Life Technologies) with 0.5 mg/ml collagenase D (Roche, Basel, Switzerland). For micromass culture (37), cells (2×10^5 cells/10 μl) were added to the center of each well of a 24-well plate and then incubated at 37˚C for 2 h to allow cells to adhere. To each well was then added 500 μl DMEM containing 10% FCS supplemented with IFN-γ (0, 0.4, 2, 10 ng/ml; PeproTech, Rocky Hill, NJ), TNF (0, 0.4, 2, 10 ng/ml; PeproTech), IL-17 (0, 0.4, 2, 10 ng/ml; R&D Systems), or TGF-β (0, 0.4, 2, 10 ng/ml; PeproTech). After 7 d, cells were fixed in neutralized 10% formalin, rinsed with 0.1 N HCl, followed by staining with 1% Alcian blue 8GX (Sigma-Aldrich) solution. The images were obtained on a Biorevo BZ-9000 microscope (Keyence, Osaka, Japan), and the Alcian blue$^+$ area and staining intensity were quantitated using the ImageJ software (National Institutes of Health).

Murine osteoblast primary culture

Calvarial cells were prepared by sequential digestion according to a standard method. Briefly, calvaria from 1- to 2-d-old neonates were surgically isolated, and the adherent mesenchymal tissues were trimmed. The neonatal calvaria was first digested in degradation solution containing 0.1% collagenase (Wako Pure Chemical Industries, Osaka, Japan) and 0.1% dispase (Roche) for 10 min at 37˚C with agitation. The solution was discarded to remove debris, and the remaining calvaria were further digested in the same degradation solution for 1 h at 37˚C. Cells isolated from serial digestions were suspended in α-MEM containing 10% FCS, penicillin (100 U/ml), and streptomycin (100 μg/ml) and plated at a concentration of 2×10^5 cells per well in 12-well plates. After 2 d of culture, the cells were incubated in an osteogenic medium (α-MEM supplemented with 10% FCS, 50 μg/ml ascorbic acid [Sigma-Aldrich], 10 mM β-glycerophosphate [Calbiochem, La Jolla, CA], and antibiotics) for 14 or 21 d, with the medium replaced every 3 d for the entire duration. The primary murine osteoblasts were cultured in the presence of recombinant murine IFN-γ (PeproTech) from the start of the culture, and IFN-γ was added every 3 d when the osteogenic medium was replaced. The mineralization formation of osteoblastic cells was detected using the von Kossa method and alizarin red S (sodium alizarin sulfonate) staining. For the von Kossa method, osteoblast cultures were fixed in 10% formalin for 10 min at room temperature. After rinsing, the fixed cells were exposed to bright sunlight in 5% silver nitrate solution for 30 min, followed by a 5% sodium thiosulfate wash. The mineralized nodules were visualized as dark brown or black spots. For alizarin red S staining, osteoblasts were fixed with 10% formalin for 10 min at room temperature and then stained with 1% alizarin red S (pH 4.2) for 10 min at room temperature. After washing with distilled water to remove excess dye, the mineralized nodules were seen as red spots. Cell images were captured on a GT-X770 image scanner (Seiko Epson, Nagano, Japan).

Statistical analysis

An unpaired two-tailed Student *t* test and a Mann–Whitney *U* test were used for the statistical evaluation of results. Multigroup comparisons were performed by one-way ANOVA followed by a Tukey HSD post hoc test. Incidence of ankylosis was compared using a Fisher exact test. A p value < 0.05 was considered statistically significant.

Results

Ankylosing enthesitis develops spontaneously in aged Dcir$^{-/-}$ *mice*

Enthesitis of the ankle joints of hindlimbs developed spontaneously in *Dcir*$^{-/-}$ mice of the 129/Ola × C57BL/6J background, starting at 4 mo of age (3). Enthesitis also developed in aged *Dcir*$^{-/-}$ mice after backcrossing for 9–12 generations to C57BL/6J mice (Supplemental Fig. 1A, Table I). In those animals, enthesitis was followed by the development of joint ankylosis with limited joint motion (Fig. 1A). Joint ankylosis developed in ∼20% of male *Dcir*$^{-/-}$ mice by 12 mo of age (Fig. 1B), but not in female mice (data not shown). To examine bone microstructure in the affected joints, we performed x-ray and three-dimensional (3D) μCT analyses. Aged *Dcir*$^{-/-}$ mice exhibited joint deformity associated with accelerated ossification around the joint cavity and tendon, suggesting that heterotopic ossification leads to ankylosis of the joint (Fig. 1C). H&E staining revealed entheseal cell proliferation and ligament thickening (Fig. 1D, *left*, Table I), and Safranin O/Fast Green staining revealed significant cartilage proteoglycan deposition in the proliferative entheseal tissues of the ankle joints of aged *Dcir*$^{-/-}$ mice (Fig. 1D, *right*, arrowheads, Table I). Enthesopathy was also detected in knee joints and thoracic vertebrae, as well as ankle joints, of aged *Dcir*$^{-/-}$ mice (Supplemental Fig. 1B). These results suggest that enthesitis followed by abnormal cartilage formation and heterotopic ossification leads to ankylosis of peripheral and axial joints in aged *Dcir*$^{-/-}$ mice.

Dcir$^{-/-}$ *mice exhibit a mild increase of bone mass*

We also investigated the bone architectures of young *Dcir*$^{-/-}$ mice. A histomorphometric analysis of the tibia distal metaphysis revealed increases in both osteoclastic and osteoblastic parameters (Supplemental Fig. 2A). μCT analysis showed that *Dcir*$^{-/-}$ mice at 8 wk of age had a mild increase of bone mass in the femur, accompanied by increases in bone volume and trabecular number (Fig. 2A). Remarkably, a dynamic histomorphometric analysis revealed a higher mineral apposition rate and bone formation rate per unit of trabecular bone surface in *Dcir*$^{-/-}$ mice (Fig. 2B). Thus, DCIR deficiency resulted in higher bone turnover, in which bone formation was dominant over bone destruction. However, DCIR expression was undetectable in osteoblasts (data not shown), and differentiation and mineralization activity were similar between the WT and *Dcir*$^{-/-}$ osteoblasts in vitro (Supplemental Fig. 2B, 2C). Additionally, mRNA expression of RANKL (*Tnfsf11*), a differentiation factor of osteoclasts, and OPG (*Tnfrsf11b*), a decoy receptor for RANKL, were comparable upon stimulation with 1,25-$(OH)_2$ vitamin D_3, PGE_2, and ascorbic acid (Supplemental Fig. 2D), suggesting that DCIR deficiency had no direct effect on osteoblasts.

Rag2 *deficiency suppresses the development of ankylosis and increase in bone volume in* Dcir$^{-/-}$ *mice*

Because *Dcir*$^{-/-}$ mice developed autoimmune-like symptoms due to overexpansion of DCs (3), we examined the possibility that this

Table I. Histopathological findings in ankle joints of aged $Dcir^{-/-}$ mice

Genotype	Incidence, % (Affected/Total)			
	Enthesitis	Tendon or Ligament Thickening	Cartilage Formation	Bone Fusion
WT	11.8 (2/17)	5.9 (1/17)	5.9 (1/17)	0 (0/17)
$Dcir^{-/-}$	57.9 (11/19)**	52.6 (10/19)***	36.8 (7/19)*	36.8 (7/19)**
$Rag2^{-/-}Dcir^{-/-}$	0 (0/19)†††	10.5 (2/19)†	5.3 (1/19)†	0 (0/19)††
$Tnf^{-/-}Dcir^{-/-}$	0 (0/13)†††	7.7 (1/13)†	0 (0/13)†	0 (0/13)†
$Il17a^{-/-}Dcir^{-/-}$	35.3 (6/17)	58.8 (10/17)***	52.9 (9/17)***	41.2 (9/17)***
$Ifng^{-/-}Dcir^{-/-}$	23.5 (4/17)†	23.5 (4/17)	0 (0/17)††	0 (0/17)††

Paraffin sections of ankle joints were prepared from 10- to 12-mo-old WT (n = 17), $Dcir^{-/-}$ (n = 19), $Rag2^{-/-}Dcir^{-/-}$ (n = 19), $Tnf^{-/-}Dcir^{-/-}$ (n = 13), $Il17a^{-/-}Dcir^{-/-}$ (n = 17), and $Ifng^{-/-}Dcir^{-/-}$ (n = 17) mice and stained with H&E. The incidence of enthesitis, tendon or ligament thickening, cartilage formation, and bone fusion in each genotype are shown.

*$p < 0.05$, **$p < 0.01$, ***$p < 0.005$ (versus WT), $^{\dagger}p < 0.05$, $^{\dagger\dagger}p < 0.01$, $^{\dagger\dagger\dagger}p < 0.005$ (versus $Dcir^{-/-}$) by Fisher exact test.

abnormality of the immune system is involved in the development of bone abnormalities. Ankylosis of ankle joints was completely suppressed in $Rag2^{-/-}Dcir^{-/-}$ mice, even at 1 y of age (Fig. 3A). Histopathological analysis confirmed that entheses of aged $Rag2^{-/-}Dcir^{-/-}$ mice were normal, without any inflammation or new cartilage formation (Fig. 3B, Table I). Moreover, μCT analysis revealed that the increase in bone volume was also abolished in $Rag2^{-/-}Dcir^{-/-}$ mice (Fig. 3C). These results suggest that the ankylosing enthesitis and the increased bone mass in $Dcir^{-/-}$ mice are caused by the disturbance of the immune system resulting from DCIR deficiency.

IFN-γ–producing T cells are expanded in $Dcir^{-/-}$ *mice*

Because *Rag2* deficiency abolished the bone abnormalities in $Dcir^{-/-}$ mice, we assumed that T cells and/or B cells were responsible for the ankylosing enthesitis and increased bone mass. However, *Clec4a2* mRNA was barely detectable in B cells, but not in T cells (3), and $Dcir^{-/-}$ B cells expressed levels of B cell–specific surface markers, such as IgM, IgD, CD5, and CD43, comparable to those on WT B cells (data not shown). Therefore, we examined the effect of *Dcir* deficiency on the activation and differentiation of T cells. The proportion of IFN-γ^{+}CD4^{+} and IFN-γ^{+}CD8^{+} T cells in popliteal lymph nodes (LNs) from 12-wk-old $Dcir^{-/-}$ mice was larger than those in WT mice, whereas the proportion of IL-17^{+}CD4^{+} T cells was similar (Fig. 4A, 4B). The numbers of IFN-γ^{+}CD4^{+} and IFN-γ^{+}CD8^{+} T cells infiltrating into the ankle joint were also elevated in $Dcir^{-/-}$ mice, whereas the number of IL-17^{+}CD4^{+} T cells was not (Fig. 4C). The concentration of IFN-γ and TNF was higher in joint extracts from $Dcir^{-/-}$ mice than those from WT mice

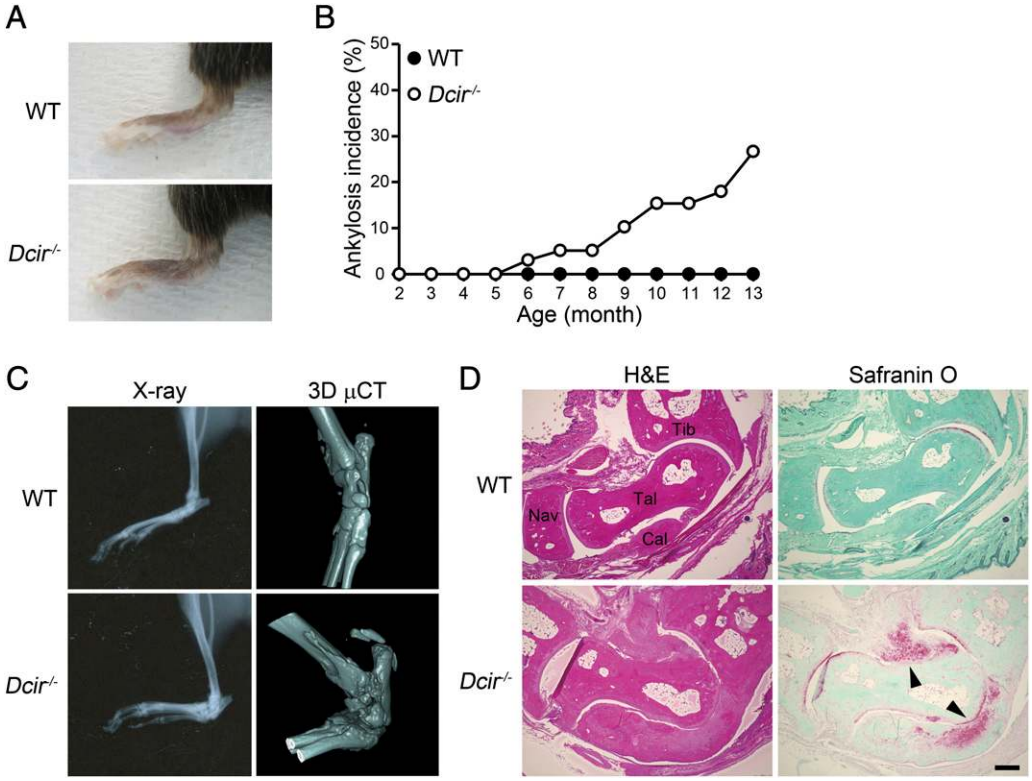

FIGURE 1. Male $Dcir^{-/-}$ mice spontaneously develop joint ankylosis with age. (**A**) Hindpaws of WT and $Dcir^{-/-}$ mice with ankylosis. Representative macroscopic images of 12-mo-old mice are shown. (**B**) Incidence of ankylosis in WT and $Dcir^{-/-}$ mice. Groups of age-matched WT (n = 26) and $Dcir^{-/-}$ (n = 30) mice were monitored once a week for 12 mo. Data are representative of three independent groups. (**C**) Radiographic and 3D μCT images of ankle joints from 12-mo-old WT and $Dcir^{-/-}$ mice. Representative images are shown. (**D**) Histopathologies of ankle joints from 12-mo-old WT and $Dcir^{-/-}$ mice. Formalin-fixed and paraffin-embedded sections of ankle joints were stained with H&E (*left*) or Safranin O/Fast Green (*right*). Representative sections are shown. Arrowheads indicate cartilage matrix deposition. Scale bar, 300 μm. Cal, calcaneum; Nav, navicular; Tib, tibia; Tal, talus.

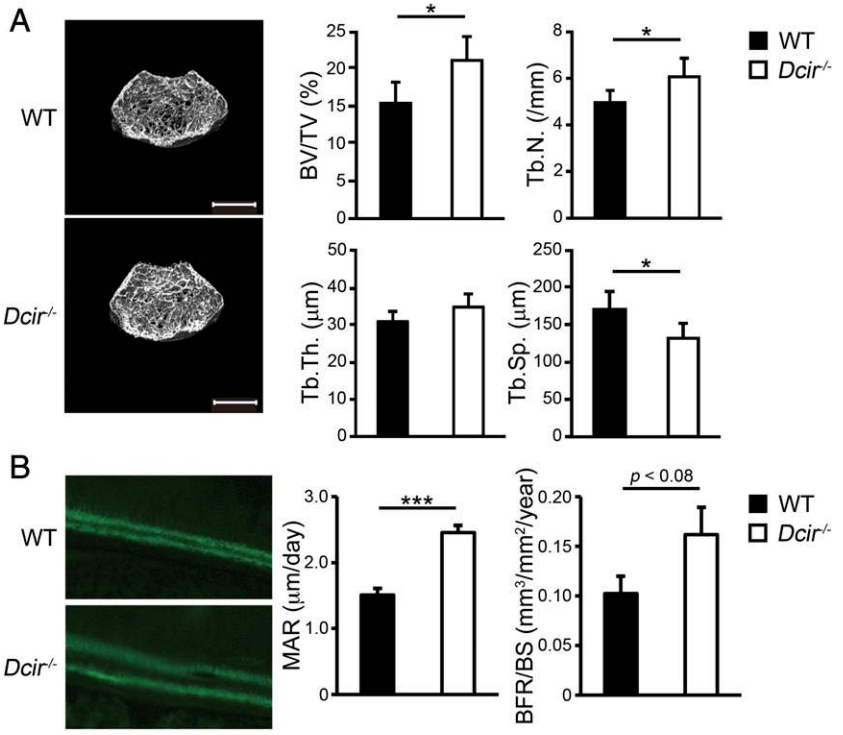

FIGURE 2. $Dcir^{-/-}$ mice exhibit an increase in bone volume. (**A**) μCT images (*left*) and bone parameters (*right*) of femoral trabeculae in 8-wk-old WT and $Dcir^{-/-}$ mice ($n = 5$). Bone volume density (bone volume/tissue volume; BV/TV), trabecular number (Tb.N), trabecular thickness (Tb. Th.), and trabecular separation (Tb.Sp.) are shown. Representative images are shown. Scale bar, 1 mm. (**B**) In vivo bone formation in 8-wk-old WT ($n = 8$) and $Dcir^{-/-}$ mice ($n = 7$) was determined by calcein double-labeling. Calcein staining (*left*, original magnification ×40) and mineral apposition rate (MAR) and bone formation rate (BFR/bone surface [BS]) (*right*) are shown. Data from two independent experiments are pooled. Values are mean ± SEM. $*p < 0.05$, $***p < 0.005$ by unpaired two-tailed Student *t* test.

(Fig. 4D). Additionally, T cells in the peripheral blood and the brachial and axillary, but not mesenteric, LNs of $Dcir^{-/-}$ mice secreted higher levels of IFN-γ, and the serum concentration of IFN-γ in $Dcir^{-/-}$ mice tended to be higher than that of WT mice (Fig. 4E, 4F, Supplemental Fig. 3). Thus, these observations show that IFN-γ–producing T cells are preferentially expanded in $Dcir^{-/-}$ mice, forming an IFN-γ–dominant cytokine milieu.

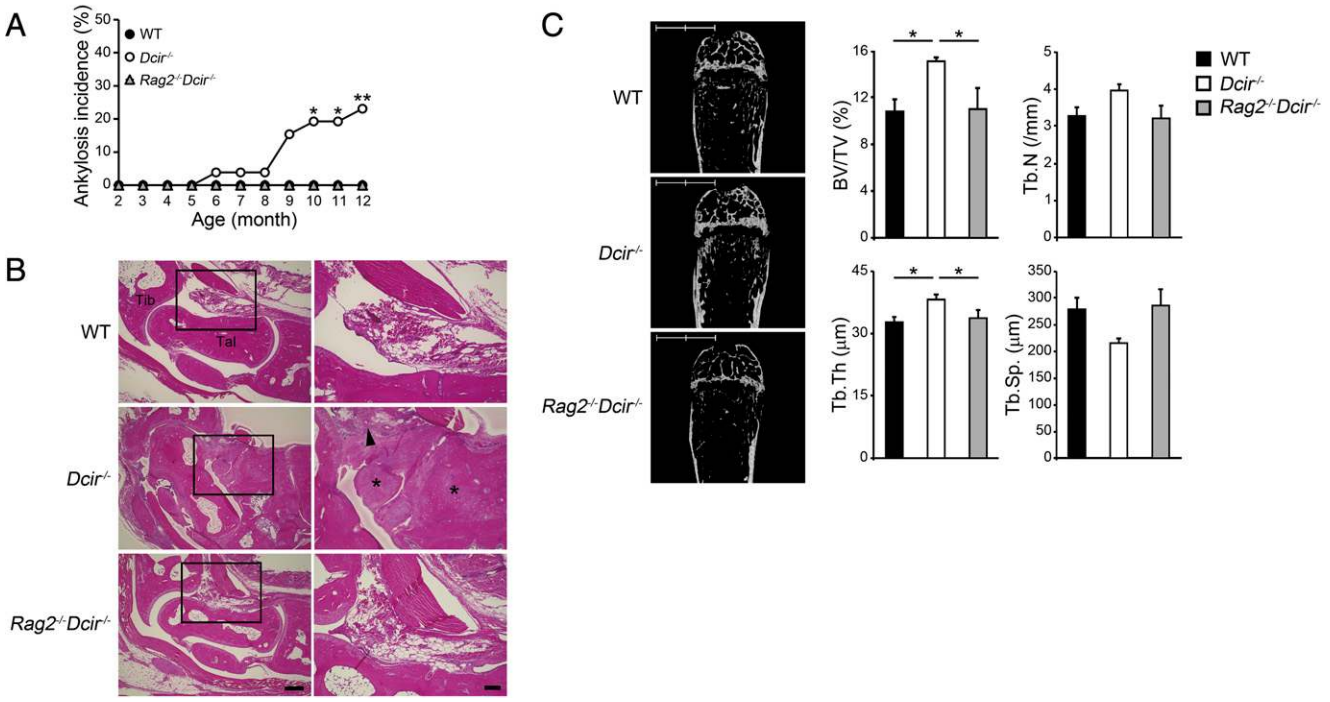

FIGURE 3. Ankylosis and increase of bone volume are suppressed in *Rag2*-deficient $Dcir^{-/-}$ mice. (**A**) Incidence of ankylosis in male WT, $Dcir^{-/-}$, and $Rag2^{-/-}Dcir^{-/-}$ mice. Groups of age-matched WT ($n = 26$), $Dcir^{-/-}$ ($n = 26$), and $Rag2^{-/-}Dcir^{-/-}$ ($n = 27$) mice were monitored once a week for 12 mo. Data are representative of two independent groups. (**B**) H&E staining of hindpaws from 12-mo-old WT, $Dcir^{-/-}$, and $Rag2^{-/-}Dcir^{-/-}$ mice. Representative sections from each genotype are shown. *Right panels* are magnified views (original magnification ×10) of regions of the *left panels* (original magnification ×4). Arrowhead indicates ligament thickening, and asterisks indicate new cartilage formation. Scale bars, 300 μm (*left*) and 100 μm (*right*). (**C**) μCT images (*left*) and bone parameters (*right*) of the distal sites of femurs in 9-wk-old WT, $Dcir^{-/-}$, and $Rag2^{-/-}Dcir^{-/-}$ mice ($n = 4$–6). Scale bars, 2 mm. Values are mean ± SEM. $*p < 0.05$ by one-way ANOVA with Tukey HSD post hoc test. BV/TV, bone volume/tissue volume; Tb.N, trabecular number; Tb.Sp., trabecular separation; Tb.Th., trabecular thickness.

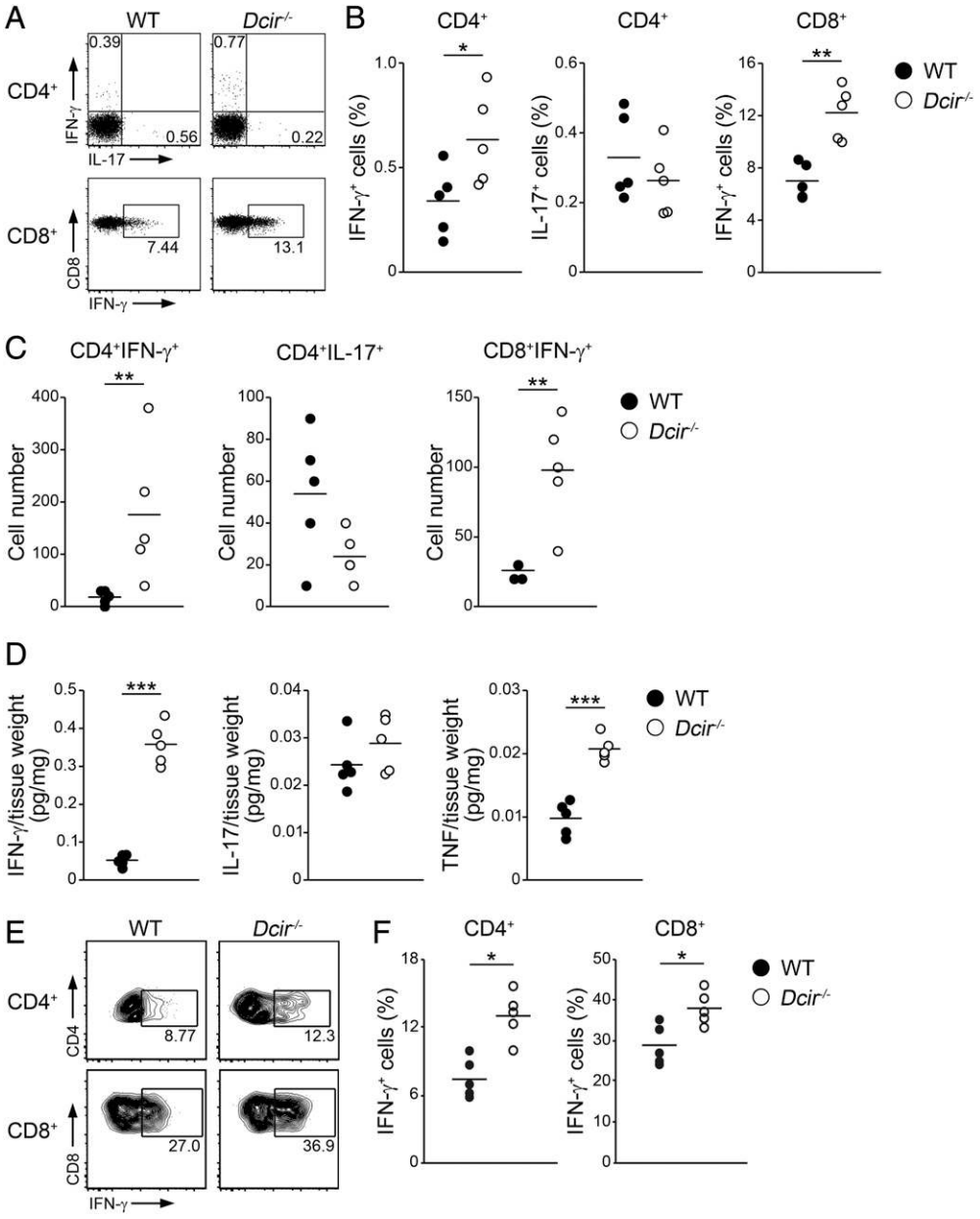

FIGURE 4. IFN-γ–producing T cells accumulate in LNs and joints of *Dcir*$^{-/-}$ mice. (**A** and **B**) Frequency of IFN-γ$^+$ or IL-17$^+$ cells in CD4$^+$ and CD8$^+$ T cells from popliteal LNs of 12-wk-old WT and *Dcir*$^{-/-}$ mice (n = 5 each). Popliteal LN cells were analyzed by intracellular staining (gated on CD3$^+$ CD4$^+$ and CD3$^+$CD8$^+$ cells). (**C**) Number of joint-infiltrating cells producing IFN-γ and IL-17 in 12-wk-old WT and *Dcir*$^{-/-}$ mice (n = 5 each). Cells were isolated from ankle joints and analyzed by intracellular staining (gated on CD45$^+$CD3$^+$CD4$^+$ and CD45$^+$CD3$^+$CD8$^+$ cells). (**D**) Cytokine levels in the joints of 16-wk-old WT and *Dcir*$^{-/-}$ mice (n = 5 each). The concentrations of IFN-γ, IL-17, and TNF in the homogenized lysates of ankle joints were determined by ELISA. (**E** and **F**) Frequency of IFN-γ$^+$ cells in CD4$^+$ and CD8$^+$ T cells from peripheral blood of 12-wk-old WT and *Dcir*$^{-/-}$ mice (n = 5 each). Peripheral blood cells were analyzed by intracellular staining (gated on CD3$^+$CD4$^+$ and CD3$^+$CD8$^+$ cells). Numbers in (A) and (E) denote the percentage of IFN-γ$^+$ cells within gated population. Each symbol represents an individual mouse, and small horizontal lines indicate the mean. Data are representative of three (A–C) or two (D–F) independent experiments. $*p < 0.05$, $**p < 0.01$, $***p < 0.005$ by Mann–Whitney U test.

Dcir$^{-/-}$ *DCs promote the differentiation of IFN-γ–producing T cells*

To investigate the mechanism by which IFN-γ production is enhanced in *Dcir*$^{-/-}$ mice, we analyzed the expression of activation markers on *Dcir*$^{-/-}$ DCs. The mean fluorescence intensity of CD86, CD40, and MHC class II expression was significantly higher on CD11c$^+$ DCs from popliteal LNs of *Dcir*$^{-/-}$ mice than on those from WT mice (Fig. 5A), indicating that *Dcir*$^{-/-}$ DCs are activated under physiological conditions. Next, to examine the effect of *Dcir*$^{-/-}$ DCs on T cell differentiation, we cocultured purified splenic DCs from WT and *Dcir*$^{-/-}$ mice with WT T cells, and then measured the proliferation and cytokine production from T cells. The number of T cells was significantly higher after coculture with *Dcir*$^{-/-}$ DCs than after coculture with WT DCs (data not shown). Furthermore, the frequency of IFN-γ–producing T cells and the concentration of IFN-γ in the culture medium were higher in coculture with *Dcir*$^{-/-}$ DCs, whereas there was no difference in the proportion of IL-17$^+$ T cells or the levels of IL-17 secretion (Fig. 5B–D). Thus, DCs isolated from *Dcir*$^{-/-}$ mice promote proliferation of IFN-γ–producing T cells and production of IFN-γ.

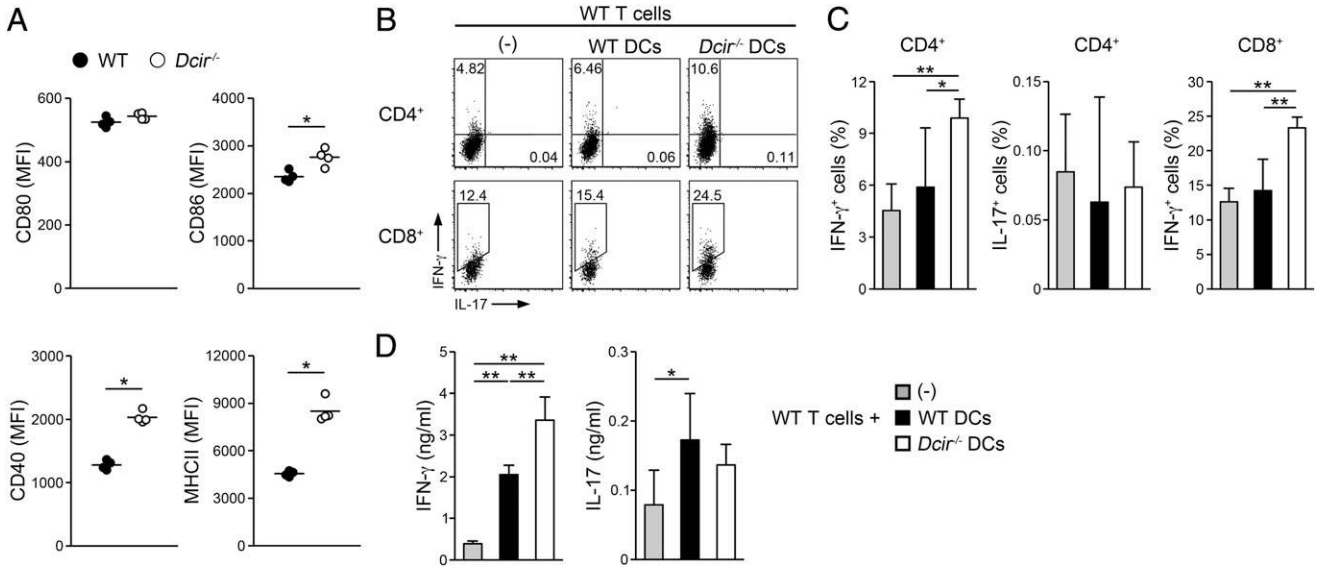

FIGURE 5. *Dcir*$^{-/-}$ DCs promote IFN-γ production by T cells. (**A**) Cell-surface expression of the costimulatory molecules and MHC class II on DCs isolated from popliteal LNs of 16-wk-old WT and *Dcir*$^{-/-}$ mice ($n = 4$). Mean fluorescence intensity (MFI) of CD80, CD86, CD40, and MHC class II in CD11c$^+$ DCs was determined by flow cytometric analysis. Each symbol represents an individual mouse, and small horizontal lines indicate the mean. (**B** and **C**) The frequency of IFN-γ$^+$ and IL-17$^+$ cells among CD4$^+$ and CD8$^+$ T cells after coculture with WT or *Dcir*$^{-/-}$ DCs. Splenic CD11c^{hi} DCs (2×10^4) were isolated from WT or *Dcir*$^{-/-}$ mice and cocultured with WT Thy1.2$^+$ T cells (2×10^5) in the presence of soluble anti-CD3 Ab (1 μg/ml) for 3 d ($n = 5$ each). Cells were analyzed by flow cytometry (gated on CD3$^+$CD4$^+$ and CD3$^+$CD8$^+$ cells). Numbers in dot plots in (B) denote the percentage of the gated population. (**D**) Concentrations of IFN-γ and IL-17 in coculture supernatants were determined by ELISA. Data are representative of two (A) or three (B–D) independent experiments. Values are mean ± SD. *$p < 0.05$, **$p < 0.01$ by Mann–Whitney *U* test or one-way ANOVA with Tukey HSD post hoc test.

IFN-γ is a pathogenic factor that causes ankylosis and increase of bone volume in Dcir$^{-/-}$ *mice*

The IL-23/IL-17 axis and TNF have been implicated in the pathogenesis of ankylotic changes (23–27). To dissect the roles of cytokines in the development of ankylosis in *Dcir*$^{-/-}$ mice, we intercrossed *Dcir*$^{-/-}$ mice with *Ifng*$^{-/-}$, *Il17a*$^{-/-}$, and *Tnf*$^{-/-}$ mice. Although disease onset age seemed to be different as shown in Figs. 1B, 3A, and 6A, we consistently observed that 20% of *Dcir*$^{-/-}$ mice developed joint ankylosis by 12 mo of age (Fig. 6A), and there were no significant statistical differences in the incidence of ankylosis in *Dcir*$^{-/-}$ mice at 4–6 mo of age (Figs. 1B, 6A: $p = 0.25$, 0.25, and 0.17 at 4, 5, and 6 mo of age, respectively; Figs. 3A, 6A: $p = 0.28$, 0.28, and 0.21, respectively; Fisher exact test). The development of ankylosis was completely suppressed in *Ifng*$^{-/-}$*Dcir*$^{-/-}$ and *Tnf*$^{-/-}$*Dcir*$^{-/-}$ mice, but not in *Il17a*$^{-/-}$*Dcir*$^{-/-}$ mice (Fig. 6A). Histopathological analysis revealed no inflammatory lesions in the enthesis of *Tnf*$^{-/-}$*Dcir*$^{-/-}$ mice (Fig. 6B). Although the incidence of enthesitis in *Ifng*$^{-/-}$*Dcir*$^{-/-}$ mice was greatly reduced, mild enthesitis and ligament thickening were still observed in some *Ifng*$^{-/-}$*Dcir*$^{-/-}$ mice (Table I). In contrast, entheseal cell proliferation and bone abnormalities were observed in the joints of *Il17a*$^{-/-}$*Dcir*$^{-/-}$ mice, similar to the case of *Dcir*$^{-/-}$ mice, indicating that IL-17 is dispensable for the pathogenesis of ankylosing enthesitis in *Dcir*$^{-/-}$ mice (Fig. 6B, arrowhead and asterisk, Table I). Thus, these results indicate that TNF and IFN-γ play important roles in the pathogenesis of ankylosis in *Dcir*$^{-/-}$ mice. Furthermore, μCT analysis of *Ifng*$^{-/-}$*Dcir*$^{-/-}$ mice revealed that aberrant bone formation was suppressed in these mice, suggesting that the increase of bone volume is also caused by aberrant systemic IFN-γ production in *Dcir*$^{-/-}$ mice (Fig. 6C).

Chondrocyte proliferation and differentiation and osteoblast differentiation are promoted by IFN-γ

Because IFN-γ is suggested to be involved in joint ankylosis and increased bone volume, we examined the effects of IFN-γ on chondrogenesis and osteoblastogenesis. Because the expression of DCIR was not detected in osteoblasts, and because mineralization, gene expressions responsible for osteoblast differentiation and function, and responses to osteoblast stimulators were comparable between WT and *Dcir*$^{-/-}$ cells (data not shown, Supplemental Fig. 2B–D), we used primary chondrocytes and osteoblasts from WT mice for these experiments. The effects of IFN-γ on chondrogenesis were examined using micromass culture of murine primary chondrocytes (37). Consistent with previous reports (38, 39), TNF and IL-17 suppressed Alcian blue$^+$ proteoglycan deposition in cultures (Fig. 7A, 7B). In contrast, IFN-γ increased proteoglycan deposition in a dose-dependent manner, similarly to TGF-β, which induces proliferation and differentiation of chondrocytes from mesenchymal stem cells (40) (Fig. 7A, 7B). IFN-γ elicited the expression of proliferating cell nuclear Ag (*Pcna*), sex-determining region Y–box 9 (*Sox9*; a transcription factor that regulates chondrocyte differentiation), and type II collagen (*Col2a1*; a cartilage matrix protein) in chondrocytes, but suppressed the expression of matrix metalloproteinase-3 (*Mmp3*; an enzyme that degrades collagens and proteoglycans) (Fig. 7C). As in chondrocytes, in calvarial osteoblast primary cultures, exogenous IFN-γ facilitated osteoblast-induced Ca^{2+} deposition and induced expression of osteogenic genes in a dose-dependent manner (Fig. 7D, 7E). These results indicate that IFN-γ promotes chondrogenesis and osteoblastogenesis by promoting proliferation, differentiation, and extracellular matrix production.

Discussion

Previously, we showed that DCIR contributes to immune homeostasis by regulating DC differentiation and proliferation (3). In this study, we showed that DCIR also plays important roles in bone homeostasis by regulating the production of IFN-γ, which we identified as a potent osteogenic factor that promotes both chondrogenesis and osteoblastogenesis.

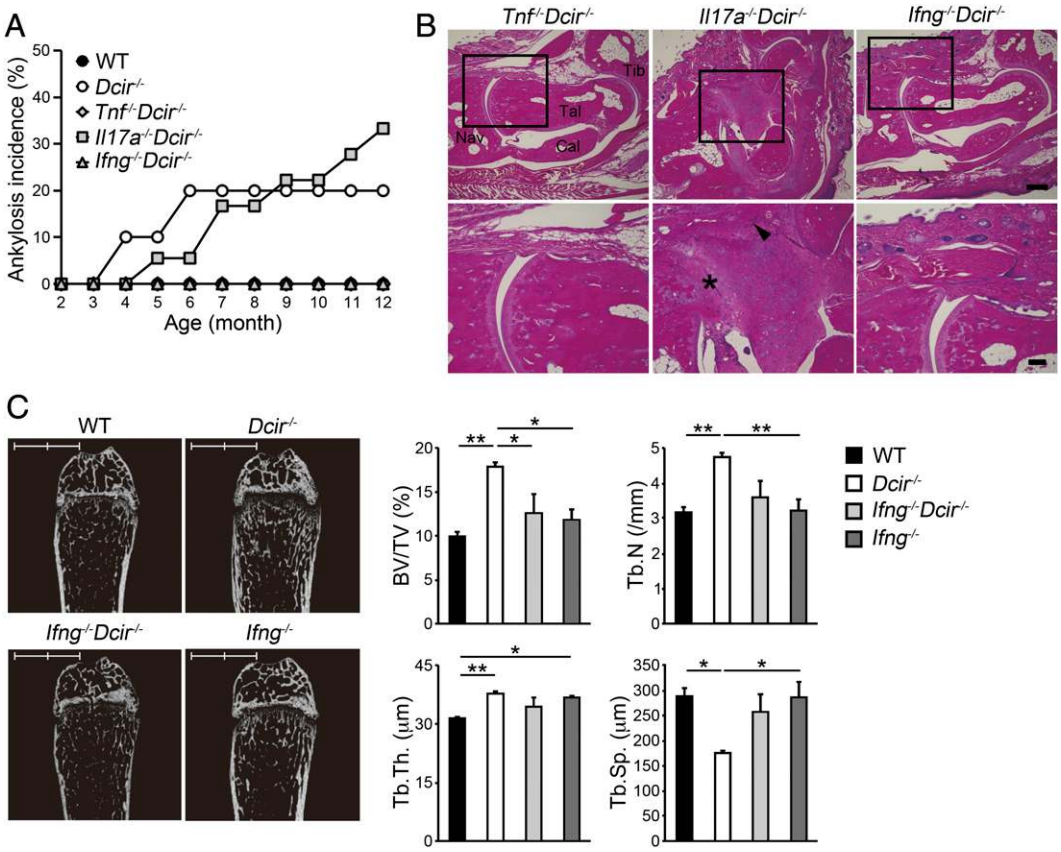

FIGURE 6. IFN-γ deficiency prevents the development of ankylosis and increased bone mass in $Dcir^{-/-}$ mice. (**A**) Incidence of ankylosis in cytokine-deficient $Dcir^{-/-}$ mice. Groups of age-matched WT (n = 10), $Dcir^{-/-}$ (n = 10), $Tnf^{-/-}Dcir^{-/-}$ (n = 18), $Il17a^{-/-}Dcir^{-/-}$ (n = 18), and $Ifng^{-/-}Dcir^{-/-}$ (n = 20) male mice were monitored once a week for 12 mo for the development of ankylosis. (**B**) Histopathologies in ankle joints of aged $Tnf^{-/-}Dcir^{-/-}$, $Il17a^{-/-}Dcir^{-/-}$, and $Ifng^{-/-}Dcir^{-/-}$ mice. Representative sections of H&E staining from each genotype are shown. *Lower panels* are magnified views (original magnification ×10) of the *upper panels* (original magnification ×4). The arrowhead indicates entheseal cell proliferation, and the asterisks indicate new cartilage formation and bone fusion. Scale bars, 300 μm (*upper*) and 100 μm (*lower*). (**C**) μCT images (*left*) and bone parameters (*right*) of the distal sites of femurs in 9-wk-old WT, $Dcir^{-/-}$, $Ifng^{-/-}Dcir^{-/-}$, and $Ifng^{-/-}$ mice (n = 4-5). Scale bars, 2 mm. Values are mean ± SEM. $*p < 0.05$, $**p < 0.01$ by one-way ANOVA with Tukey HSD post hoc test. BV/TV, bone volume/tissue volume; Tb.N, trabecular number; Tb.Sp., trabecular separation; Tb.Th., trabecular thickness.

$Dcir^{-/-}$ mice develop enthesitis, joint ankylosis, and mild increase of bone volume. We showed that these enthesitis and bone abnormalities in $Dcir^{-/-}$ mice are abolished by *Rag2* deficiency, suggesting involvement of an immune-mediated mechanism in pathogenesis. Because enthesitis was completely suppressed in $Tnf^{-/-}Dcir^{-/-}$ mice, TNF may play a major role in the development of enthesitis. Indeed, transgenic mice overexpressing TNF spontaneously develop enthesitis (41, 42) and ankylosis of joints (43). Following the entheseal inflammation, ankylotic changes of joints developed. Joint ankylosis was completely suppressed by *Tnf* and *Ifng* deficiency, but not by *Il17* deficiency, suggesting the involvement of TNF and IFN-γ, but not IL-17, in the development of ankylosing enthesitis in $Dcir^{-/-}$ mice. Consistent with our observation, systemic IL-17 overexpression does not induce ankylotic changes (44). In contrast, systemic IL-23 overexpression causes entheseal inflammation and other symptoms characteristics of human spondyloarthritis (44). IL-23 acts on newly identified entheseal T cells that produce IL-22, causing new bone formation (44). Systemic IL-23 also increases $CD11b^+$ cells in bone marrow and spleen (45), and IL-23 regulates myeloid cell differentiation via crosstalk with ITAM-coupled receptors (46). Although the role of IL-23 on myeloid cell differentiation is poorly understood, these findings raise the possibility that IL-23 may also be involved in the development of ankylosing enthesitis by acting on myeloid cells in mice lacking DCIR–ITIM pathways, which counterbalance ITAM-mediated signals. Because IFN-γ deficiency did not completely suppress enthesitis, IFN-γ may be dispensable for the development of enthesitis. Instead, IFN-γ may induce ankylotic changes, because IFN-γ promoted chondrocyte differentiation and proliferation, as well as osteoblast differentiation and activation, in vitro (18). A similar pathogenic role for IFN-γ has been proposed in proteoglycan-induced spondylitis (47) and spontaneous arthritis in male DBA/1 mice (48), which develop enthesitis and ankylosis. Increased bone volume in $Dcir^{-/-}$ mice was also suppressed in $Ifng^{-/-}Dcir^{-/-}$ mice, suggesting that IFN-γ plays an important role in the regulation of systemic bone metabolism. Consistent with our observations, bone mineral density is reduced in $Ifngr1^{-/-}$ mice (49, 50).

We showed that IFN-γ promotes chondrocyte differentiation and proliferation via induction of *Pcna*, *Sox9,* and *Col2a1* expression, thereby increasing extracellular matrix deposition. IFN-γ also induced osteoblast differentiation by inducing *Runx2*, *Osterix*, *Alp*, and *Bglap*, causing enhanced Ca^{2+} deposition in osteoblast culture. It was reported, however, that IFN-γ rather inhibits the proliferation and proteoglycan synthesis of chondrocytes in cultures (51). The reason for this discrepancy is not completely clear, but different culture conditions might have affected the results: most previous studies used chondrocyte monolayer cultures, whereas we used a high-density micromass culture system, which provides the 3D environment required for

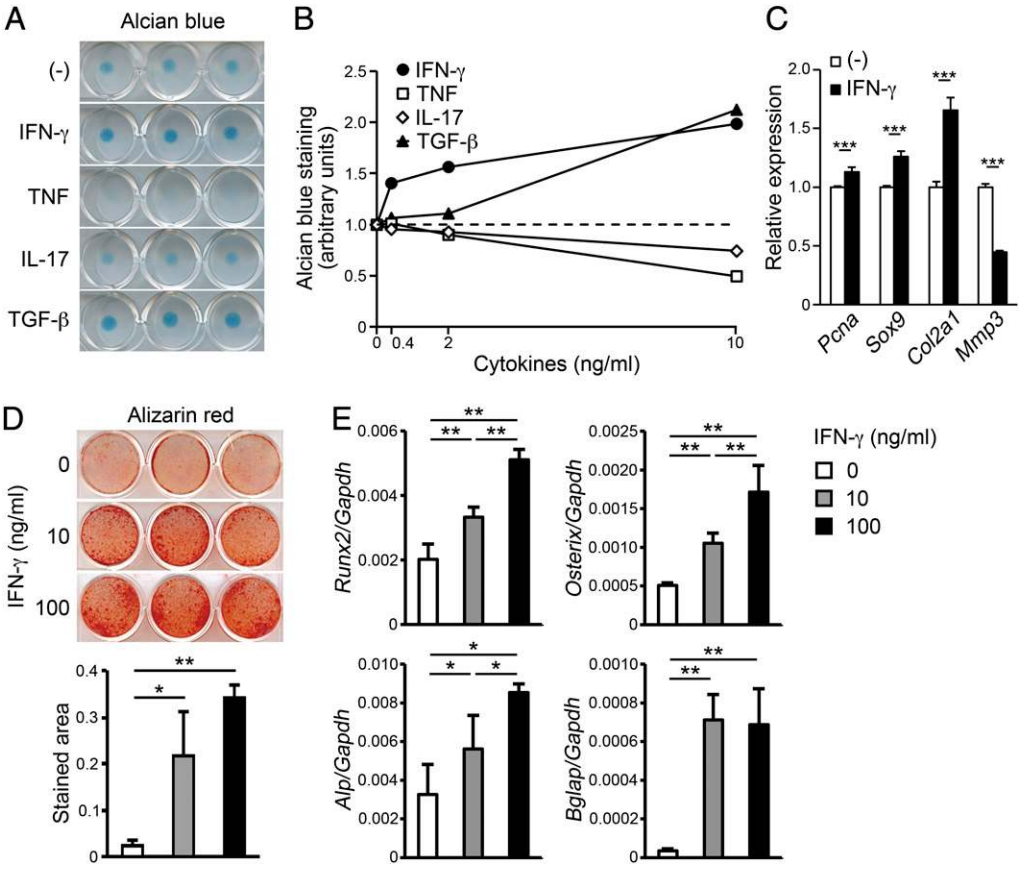

FIGURE 7. IFN-γ promotes matrix deposition in primary-cultured chondrocytes and osteoblasts. (**A**) Alcian blue staining of primary chondrocytes in the presence of IFN-γ, IL-17, TNF, or TGF-β (10 ng/ml each). Murine chondrocytes were prepared from costal cartilage of WT newborn mice and then subjected to micromass cultures for 7 d. (**B**) Quantitation of Alcian blue staining using ImageJ. Murine chondrocytes were cultured in the presence of IFN-γ, IL-17, TNF, or TGF-β (0, 0.4, 2, or 10 ng/ml) for 7 d. (**C**) Chondrogenic mRNA expressions in IFN-γ–treated chondrocytes. Total mRNA was extracted from primary chondrocytes with or without IFN-γ (10 ng/ml) on day 7. The levels of *Pcna*, *Sox9*, *Col2a1*, and *Mmp3* mRNAs were determined by real-time PCR. mRNA levels were normalized to *Actb*. (**D**) Alizarin red staining of primary osteoblasts supplemented with recombinant IFN-γ (0, 10, 100 ng/ml). Murine osteoblasts were prepared from calvaria of WT newborn mice and cultured for 14 d. The total area of alizarin red staining was analyzed using ImageJ. (**E**) Osteogenic gene expression in the treatment of IFN-γ at 14 d culture. The levels of *Runx2*, *Osterix*, *Alp*, and *Bglap* mRNAs were determined by real-time PCR. mRNA levels were normalized to *Gapdh*. Data are representative of two (B and C) or three (A, D, and E) independent experiments. Values are mean ± SD of triplicate cultures. $*p < 0.05$, $**p < 0.01$, $***p < 0.005$ by unpaired two-tailed Student *t* test or one-way ANOVA with Tukey HSD post hoc test.

proliferation, differentiation, and maturation of chondrocytes to mimic in vivo chondrogenesis (37). Based on the results obtained in the refined culture system, we propose that IFN-γ is a promoting factor for chondrogenesis, which causes joint ankylosis. Because DCIR expression was undetectable in osteoblasts and chondrocytes, it is unlikely that DCIR directly regulates proliferation and differentiation of mesenchymal cells. However, DCIR deficiency may alter the systemic cytokine milieu that affects differentiation and function of mesenchymal cells. Therefore, it is also possible that *Dcir*-deficient environment indirectly affects the response of these mesenchymal cells to IFN-γ in vivo.

It was reported that IFN-γ directly inhibits osteoclastogenesis by suppressing RANKL signaling via TNFR-associated factor 6 degradation (18). Unexpectedly, we observed that osteoclastogenesis is enhanced in $Dcir^{-/-}$ mice. Regarding this, it was reported that IFN-γ indirectly promotes bone resorption in vivo by inducing secretion of osteoclastogenic factors, such as TNF and RANKL, from T cells (52). Thus, these observations suggest that the indirect effects of IFN-γ dominate the direct effect of IFN-γ on osteoclastogenesis in $Dcir^{-/-}$ mice or DCIR may directly inhibit osteoclastogenesis. Because phosphatases, such as SHP-1 and SHIP, negatively regulate osteoclastgenesis by counterbalancing the ITAM-mediated signaling, which is essential for osteoclast differentiation (53, 54), and a phosphorylated peptide covering the ITIM sequence of DCIR binds to SHP-1, DCIR may regulate osteoclastogenesis by preferentially recruiting the phosphatase into the ITIM of DCIR (5). Although further studies are needed, an increased number of osteoclasts in $Dcir^{-/-}$ mice can be explained by the direct regulation of osteoclastogenesis via the DCIR/ITIM/phosphatase axis. Nonetheless, we observed ankylosis and bone volume increase in $Dcir^{-/-}$ mice, suggesting that enhancement of osteogenic activity by IFN-γ dominates osteoclast activation in $Dcir^{-/-}$ mice. In support for this notion, the in vivo bone formation rate was much enhanced in $Dcir^{-/-}$ mice.

IFN-γ–producing $CD4^+$ and $CD8^+$ T cell populations were increased in LNs, peripheral blood, and joints of $Dcir^{-/-}$ mice, and serum IFN-γ levels tended to be elevated in these mice. Furthermore, we showed that $Dcir^{-/-}$ DCs support differentiation of IFN-γ–producing T cells, but not IL-17–producing T cells, in vitro. These DCs from $Dcir^{-/-}$ mice expressed elevated levels of activation markers, such as CD86, CD40, and MHC class II, under physiological conditions. Consistent with our observations, DCs from DC-specific conditional SHP-1–deficient mice express elevated levels of costimulatory molecules on DCs and preferen-

tially promote differentiation of IFN-γ–producing Th1 cells, but not Th17 cells, resulting in the development of autoimmunity (55, 56). Therefore, the defect in DCIR or its downstream effector SHP-1 causes spontaneous activation of DCs and selectively promotes IFN-γ–producing T cell differentiation by increasing expression of costimulatory molecules, resulting in the induction of excess bone formation and increase of bone volume. In particular, because IFN-γ production is significantly elevated in inflamed joints, enthesitis may promote chondrogenesis and osteogenesis around entheseals, causing ankylotic changes of joints. We also showed that bone volume is increased in young *Dcir*$^{-/-}$ mice, suggesting that IFN-γ–producing T cells expand in *Dcir*$^{-/-}$ mice even under physiological conditions. However, we cannot exclude the possibility completely that this mild increase in bone volume is a secondary effect of enthesitis, in which IFN-γ–producing T cells are expanded. It is possible that invisible inflammation at entheses in *Dcir*$^{-/-}$ mice is already present in young animals, even though their joints apparently look normal.

Joint ankylosis was developed only in 20% of male *Dcir*$^{-/-}$ mice by 12 mo of age, although the increase of bone mass and IFN-γ–producing T cells was observed in almost all *Dcir*$^{-/-}$ mice. These findings suggest that additional factors, such as environmental cues, may be required for the development of ankylosis. In fact, mechanical stress at the enthesis and/or bacterial infections have been implicated in the pathogenesis of human AS (57, 58). The higher incidence of ankylotic change in male *Dcir*$^{-/-}$ mice than in female mice is similar to the prevalence ratio in human AS patients (59). Elevated levels of androgen dehydroepiandrosterone, which can stimulate Th1 response, have been reported in male patients with AS, suggesting that a sex steroid hormone may be a determinant of male/female difference (60). However, the precise roles of sex steroids in the pathogenesis of AS remain to be elucidated.

Despite intensive studies, it is still unclear how entheseal inflammation is coupled to ankylosis in AS. In this study, we showed that TNF initiates enthesitis, and that IFN-γ produced during inflammation plays an important role in the development of ankylotic changes in *Dcir*$^{-/-}$ mice. Consistent with our results, treatment with anti-TNF and nonsteroidal anti-inflammatory drugs ameliorates inflammation in AS, but these drugs cannot suppress progression of ankylotic bone changes in AS patients and animal models (61, 62). Although the pathology observed in the axial and peripheral joints of *Dcir*$^{-/-}$ mice closely resembles that of AS in humans, the etiopathogenesis of AS patients and *Dcir*$^{-/-}$ mice seems to be totally different: in contrast to *Dcir*$^{-/-}$ mice, AS is closely associated with HLA-B27 and the IL-23/IL-17 axis, and endoplasmic reticulum stress may be involved in AS pathogenesis (63). However, *Dcir*$^{-/-}$ mice may provide a disease model for the ankylotic processes of AS. Expansion of IFN-γ–producing T cells has been observed in patients with AS and in animal models (64, 65), although their pathogenic roles are yet known. Therefore, IFN-γ may also play an important role in the ankylotic process of AS in humans.

Taken together, our findings show that DCIR plays an important role in maintaining bone homeostasis. Specifically, bone formation is excessively enhanced in *Dcir*$^{-/-}$ mice, causing increased bone mass and ankylotic changes of the joints. We have shown that the development of ankylosis and increased bone mass is completely suppressed in *Rag2*$^{-/-}$*Dcir*$^{-/-}$ mice, suggesting involvement of an immune-mediated mechanism in the pathogenesis. Those pathologies were also suppressed in *Tnf*$^{-/-}$*Dcir*$^{-/-}$ and *Ifng*$^{-/-}$*Dcir*$^{-/-}$ mice, but not in *Il17*$^{-/-}$*Dcir*$^{-/-}$ mice. Furthermore, we showed that IFN-γ is responsible for the excess chondrogenesis and osteogenesis in vitro, and IFN-γ–producing T cells are selectively expanded in *Dcir*$^{-/-}$ mice. Thus, DCIR and the downstream mediator IFN-γ are important regulators of bone metabolism, and drugs that control DCIR or IFN-γ activity should be effective for treatment of bone metabolic diseases.

Acknowledgments

We thank H. Kawahara for histopathological analysis and all the members of the Iwakura Laboratory (Tokyo University of Science) for excellent animal care.

Disclosures

The authors have no financial conflicts of interest.

References

1. Osorio, F., and C. Reis e Sousa. 2011. Myeloid C-type lectin receptors in pathogen recognition and host defense. *Immunity* 34: 651–664.
2. Bates, E. E., N. Fournier, E. Garcia, J. Valladeau, I. Durand, J. J. Pin, S. M. Zurawski, S. Patel, J. S. Abrams, S. Lebecque, et al. 1999. APCs express DCIR, a novel C-type lectin surface receptor containing an immunoreceptor tyrosine-based inhibitory motif. *J. Immunol.* 163: 1973–1983.
3. Fujikado, N., S. Saijo, T. Yonezawa, K. Shimamori, A. Ishii, S. Sugai, H. Kotaki, K. Sudo, M. Nose, and Y. Iwakura. 2008. Dcir deficiency causes development of autoimmune diseases in mice due to excess expansion of dendritic cells. *Nat. Med.* 14: 176–180.
4. Kanazawa, N., T. Okazaki, H. Nishimura, K. Tashiro, K. Inaba, and Y. Miyachi. 2002. DCIR acts as an inhibitory receptor depending on its immunoreceptor tyrosine-based inhibitory motif. *J. Invest. Dermatol.* 118: 261–266.
5. Richard, M., N. Thibault, P. Veilleux, G. Gareau-Pagé, and A. D. Beaulieu. 2006. Granulocyte macrophage-colony stimulating factor reduces the affinity of SHP-2 for the ITIM of CLECSF6 in neutrophils: a new mechanism of action for SHP-2. *Mol. Immunol.* 43: 1716–1721.
6. Pao, L. I., K. Badour, K. A. Siminovitch, and B. G. Neel. 2007. Nonreceptor protein-tyrosine phosphatases in immune cell signaling. *Annu. Rev. Immunol.* 25: 473–523.
7. Meyer-Wentrup, F., D. Benitez-Ribas, P. J. Tacken, C. J. Punt, C. G. Figdor, I. J. de Vries, and G. J. Adema. 2008. Targeting DCIR on human plasmacytoid dendritic cells results in antigen presentation and inhibits IFN-α production. *Blood* 111: 4245–4253.
8. Meyer-Wentrup, F., A. Cambi, B. Joosten, M. W. Looman, I. J. de Vries, C. G. Figdor, and G. J. Adema. 2009. DCIR is endocytosed into human dendritic cells and inhibits TLR8-mediated cytokine production. *J. Leukoc. Biol.* 85: 518–525.
9. Raggatt, L. J., and N. C. Partridge. 2010. Cellular and molecular mechanisms of bone remodeling. *J. Biol. Chem.* 285: 25103–25108.
10. Takayanagi, H. 2007. Osteoimmunology: shared mechanisms and crosstalk between the immune and bone systems. *Nat. Rev. Immunol.* 7: 292–304.
11. Nakashima, T., M. Hayashi, T. Fukunaga, K. Kurata, M. Oh-Hora, J. Q. Feng, L. F. Bonewald, T. Kodama, A. Wutz, E. F. Wagner, et al. 2011. Evidence for osteocyte regulation of bone homeostasis through RANKL expression. *Nat. Med.* 17: 1231–1234.
12. Xiong, J., M. Onal, R. L. Jilka, R. S. Weinstein, S. C. Manolagas, and C. A. O'Brien. 2011. Matrix-embedded cells control osteoclast formation. *Nat. Med.* 17: 1235–1241.
13. Negishi-Koga, T., M. Shinohara, N. Komatsu, H. Bito, T. Kodama, R. H. Friedel, and H. Takayanagi. 2011. Suppression of bone formation by osteoclastic expression of semaphorin 4D. *Nat. Med.* 17: 1473–1480.
14. Pederson, L., M. Ruan, J. J. Westendorf, S. Khosla, and M. J. Oursler. 2008. Regulation of bone formation by osteoclasts involves Wnt/BMP signaling and the chemokine sphingosine-1-phosphate. *Proc. Natl. Acad. Sci. USA* 105: 20764–20769.
15. Tang, Y., X. Wu, W. Lei, L. Pang, C. Wan, Z. Shi, L. Zhao, T. R. Nagy, X. Peng, J. Hu, et al. 2009. TGF-β1-induced migration of bone mesenchymal stem cells couples bone resorption with formation. *Nat. Med.* 15: 757–765.
16. Zaidi, M. 2007. Skeletal remodeling in health and disease. *Nat. Med.* 13: 791–801.
17. Sato, K., A. Suematsu, K. Okamoto, A. Yamaguchi, Y. Morishita, Y. Kadono, S. Tanaka, T. Kodama, S. Akira, Y. Iwakura, et al. 2006. Th17 functions as an osteoclastogenic helper T cell subset that links T cell activation and bone destruction. *J. Exp. Med.* 203: 2673–2682.
18. Takayanagi, H., K. Ogasawara, S. Hida, T. Chiba, S. Murata, K. Sato, A. Takaoka, T. Yokochi, H. Oda, K. Tanaka, et al. 2000. T-cell-mediated regulation of osteoclastogenesis by signalling cross-talk between RANKL and IFN-γ. *Nature* 408: 600–605.
19. Azuma, Y., K. Kaji, R. Katogi, S. Takeshita, and A. Kudo. 2000. Tumor necrosis factor-α induces differentiation of and bone resorption by osteoclasts. *J. Biol. Chem.* 275: 4858–4864.
20. Lee, Y. M., N. Fujikado, H. Manaka, H. Yasuda, and Y. Iwakura. 2010. IL-1 plays an important role in the bone metabolism under physiological conditions. *Int. Immunol.* 22: 805–816.
21. Braun, J., and J. Sieper. 2007. Ankylosing spondylitis. *Lancet* 369: 1379–1390.
22. Dougados, M., and D. Baeten. 2011. Spondyloarthritis. *Lancet* 377: 2127–2137.

23. Australo-Anglo-American Spondyloarthritis Consortium (TASC). 2010. Genome-wide association study of ankylosing spondylitis identifies non-MHC susceptibility loci. *Nat. Genet.* 42: 123–127.
24. Braun, J., M. Bollow, L. Neure, E. Seipelt, F. Seyrekbasan, H. Herbst, U. Eggens, A. Distler, and J. Sieper. 1995. Use of immunohistologic and in situ hybridization techniques in the examination of sacroiliac joint biopsy specimens from patients with ankylosing spondylitis. *Arthritis Rheum.* 38: 499–505.
25. Spondyloarthritis Research Consortium of Canada (SPARCC)Australo-Anglo-American Spondyloarthritis Consortium (TASC)Wellcome Trust Case Control Consortium 2 (WTCCC2). 2011. Interaction between ERAP1 and HLA-B27 in ankylosing spondylitis implicates peptide handling in the mechanism for HLA-B27 in disease susceptibility. *Nat. Genet.* 43: 761–767.
26. Mei, Y., F. Pan, J. Gao, R. Ge, Z. Duan, Z. Zeng, F. Liao, G. Xia, S. Wang, S. Xu, et al. 2011. Increased serum IL-17 and IL-23 in the patient with ankylosing spondylitis. *Clin. Rheumatol.* 30: 269–273.
27. Wellcome Trust Case Control ConsortiumAustralo-Anglo-American Spondylitis Consortium (TASC)Biologics in RA Genetics and Genomics Study Syndicate (BRAGGS) Steering CommitteeBreast Cancer Susceptibility Collaboration (UK). 2007. Association scan of 14,500 nonsynonymous SNPs in four diseases identifies autoimmunity variants. *Nat. Genet.* 39: 1329–1337.
28. Diarra, D., M. Stolina, K. Polzer, J. Zwerina, M. S. Ominsky, D. Dwyer, A. Korb, J. Smolen, M. Hoffmann, C. Scheinecker, et al. 2007. Dickkopf-1 is a master regulator of joint remodeling. *Nat. Med.* 13: 156–163.
29. Lories, R. J., I. Derese, and F. P. Luyten. 2005. Modulation of bone morphogenetic protein signaling inhibits the onset and progression of ankylosing enthesitis. *J. Clin. Invest.* 115: 1571–1579.
30. Fowler, M. J., Jr., M. S. Neff, R. C. Borghaei, E. A. Pease, E. Mochan, and R. D. Thornton. 1998. Induction of bone morphogenetic protein-2 by interleukin-1 in human fibroblasts. *Biochem. Biophys. Res. Commun.* 248: 450–453.
31. Fukui, N., Y. Zhu, W. J. Maloney, J. Clohisy, and L. J. Sandell. 2003. Stimulation of BMP-2 expression by pro-inflammatory cytokines IL-1 and TNF-α in normal and osteoarthritic chondrocytes. *J. Bone Joint Surg. Am.* 85-A(Suppl. 3): 59–66.
32. Lories, R. J., I. Derese, J. L. Ceuppens, and F. P. Luyten. 2003. Bone morphogenetic proteins 2 and 6, expressed in arthritic synovium, are regulated by proinflammatory cytokines and differentially modulate fibroblast-like synoviocyte apoptosis. *Arthritis Rheum.* 48: 2807–2818.
33. Tagawa, Y., K. Sekikawa, and Y. Iwakura. 1997. Suppression of concanavalin A-induced hepatitis in IFN-$\gamma^{-/-}$ mice, but not in TNF-$\alpha^{-/-}$ mice: role for IFN-γ in activating apoptosis of hepatocytes. *J. Immunol.* 159: 1418–1428.
34. Nakae, S., Y. Komiyama, A. Nambu, K. Sudo, M. Iwase, I. Homma, K. Sekikawa, M. Asano, and Y. Iwakura. 2002. Antigen-specific T cell sensitization is impaired in IL-17-deficient mice, causing suppression of allergic cellular and humoral responses. *Immunity* 17: 375–387.
35. Taniguchi, T., M. Takata, A. Ikeda, E. Momotani, and K. Sekikawa. 1997. Failure of germinal center formation and impairment of response to endotoxin in tumor necrosis factor α-deficient mice. *Lab. Invest.* 77: 647–658.
36. Gosset, M., F. Berenbaum, S. Thirion, and C. Jacques. 2008. Primary culture and phenotyping of murine chondrocytes. *Nat. Protoc.* 3: 1253–1260.
37. Xu, Y., G. Balooch, M. Chiou, E. Bekerman, R. O. Ritchie, and M. T. Longaker. 2007. Analysis of the material properties of early chondrogenic differentiated adipose-derived stromal cells (ASC) using an in vitro three-dimensional micromass culture system. *Biochem. Biophys. Res. Commun.* 359: 311–316.
38. Goldring, M. B., M. Otero, K. Tsuchimochi, K. Ijiri, and Y. Li. 2008. Defining the roles of inflammatory and anabolic cytokines in cartilage metabolism. *Ann. Rheum. Dis.* 67(Suppl. 3): iii75–iii82.
39. Ikebe, T., M. Hirata, and T. Koga. 1988. Effects of human recombinant tumor necrosis factor-alpha and interleukin 1 on the synthesis of glycosaminoglycan and DNA in cultured rat costal chondrocytes. *J. Immunol.* 140: 827–831.
40. Li, T. F., R. J. O'Keefe, and D. Chen. 2005. TGF-β signaling in chondrocytes. *Front. Biosci.* 10: 681–688.
41. Redlich, K., B. Görtz, S. Hayer, J. Zwerina, G. Kollias, G. Steiner, J. S. Smolen, and G. Schett. 2004. Overexpression of tumor necrosis factor causes bilateral sacroiliitis. *Arthritis Rheum.* 50: 1001–1005.
42. Armaka, M., M. Apostolaki, P. Jacques, D. L. Kontoyiannis, D. Elewaut, and G. Kollias. 2008. Mesenchymal cell targeting by TNF as a common pathogenic principle in chronic inflammatory joint and intestinal diseases. *J. Exp. Med.* 205: 331–337.
43. Crew, M. D., R. B. Effros, R. L. Walford, E. Zeller, H. Cheroutre, and E. Brahn. 1998. Transgenic mice expressing a truncated *Peromyscus leucopus* TNF-α gene manifest an arthritis resembling ankylosing spondylitis. *J. Interferon Cytokine Res.* 18: 219–225.
44. Sherlock, J. P., B. Joyce-Shaikh, S. P. Turner, C. C. Chao, M. Sathe, J. Grein, D. M. Gorman, E. P. Bowman, T. K. McClanahan, J. H. Yearley, et al. 2012. IL-23 induces spondyloarthropathy by acting on ROR-γt$^+$ CD3$^+$CD4$^-$CD8$^-$ entheseal resident T cells. *Nat. Med.* 18: 1069–1076.
45. Adamopoulos, I. E., M. Tessmer, C. C. Chao, S. Adda, D. Gorman, M. Petro, C. C. Chou, R. H. Pierce, W. Yao, N. E. Lane, et al. 2011. IL-23 is critical for induction of arthritis, osteoclast formation, and maintenance of bone mass. *J. Immunol.* 187: 951–959.
46. Shin, H. S., R. Sarin, N. Dixit, J. Wu, E. Gershwin, E. P. Bowman, and I. E. Adamopoulos. 2015. Crosstalk among IL-23 and DNAX activating protein of 12 kDa-dependent pathways promotes osteoclastogenesis. *J. Immunol.* 194: 316–324.
47. Finnegan, A., M. J. Grusby, C. D. Kaplan, S. K. O'Neill, H. Eibel, T. Koreny, M. Czipri, K. Mikecz, and J. Zhang. 2002. IL-4 and IL-12 regulate proteoglycan-induced arthritis through Stat-dependent mechanisms. *J. Immunol.* 169: 3345–3352.
48. Matthys, P., R. J. Lories, B. De Klerck, H. Heremans, F. P. Luyten, and A. Billiau. 2003. Dependence on interferon-gamma for the spontaneous occurrence of arthritis in DBA/1 mice. *Arthritis Rheum.* 48: 2983–2988.
49. Duque, G., D. C. Huang, N. Dion, M. Macoritto, D. Rivas, W. Li, X. F. Yang, J. Li, J. Lian, F. T. Marino, et al. 2011. Interferon-γ plays a role in bone formation in vivo and rescues osteoporosis in ovariectomized mice. *J. Bone Miner. Res.* 26: 1472–1483.
50. Duque, G., D. C. Huang, M. Macoritto, D. Rivas, X. F. Yang, L. G. Ste-Marie, and R. Kremer. 2009. Autocrine regulation of interferon γ in mesenchymal stem cells plays a role in early osteoblastogenesis. *Stem Cells* 27: 550–558.
51. Verbruggen, G., A. M. Malfait, E. M. Veys, L. Gyselbrecht, J. Lambert, and K. F. Almqvist. 1993. Influence of interferon-γ on isolated chondrocytes from human articular cartilage. Dose dependent inhibition of cell proliferation and proteoglycan synthesis. *J. Rheumatol.* 20: 1020–1026.
52. Gao, Y., F. Grassi, M. R. Ryan, M. Terauchi, K. Page, X. Yang, M. N. Weitzmann, and R. Pacifici. 2007. IFN-γ stimulates osteoclast formation and bone loss in vivo via antigen-driven T cell activation. *J. Clin. Invest.* 117: 122–132.
53. Aoki, K., E. Didomenico, N. A. Sims, K. Mukhopadhyay, L. Neff, A. Houghton, M. Amling, J. B. Levy, W. C. Horne, and R. Baron. 1999. The tyrosine phosphatase SHP-1 is a negative regulator of osteoclastogenesis and osteoclast resorbing activity: increased resorption and osteopenia in *me^v/me^v* mutant mice. *Bone* 25: 261–267.
54. Takeshita, S., N. Namba, J. J. Zhao, Y. Jiang, H. K. Genant, M. J. Silva, M. D. Brodt, C. D. Helgason, J. Kalesnikoff, M. J. Rauh, et al. 2002. SHIP-deficient mice are severely osteoporotic due to increased numbers of hyperresorptive osteoclasts. *Nat. Med.* 8: 943–949.
55. Abram, C. L., G. L. Roberge, L. I. Pao, B. G. Neel, and C. A. Lowell. 2013. Distinct roles for neutrophils and dendritic cells in inflammation and autoimmunity in motheaten mice. *Immunity* 38: 489–501.
56. Kaneko, T., Y. Saito, T. Kotani, H. Okazawa, H. Iwamura, M. Sato-Hashimoto, Y. Kanazawa, S. Takahashi, K. Hiromura, S. Kusakari, et al. 2012. Dendritic cell-specific ablation of the protein tyrosine phosphatase Shp1 promotes Th1 cell differentiation and induces autoimmunity. *J. Immunol.* 188: 5397–5407.
57. Benjamin, M., H. Toumi, D. Suzuki, S. Redman, P. Emery, and D. McGonagle. 2007. Microdamage and altered vascularity at the enthesis-bone interface provides an anatomic explanation for bone involvement in the HLA-B27-associated spondylarthritides and allied disorders. *Arthritis Rheum.* 56: 224–233.
58. Mathieu, A., F. Paladini, A. Vacca, A. Cauli, M. T. Fiorillo, and R. Sorrentino. 2009. The interplay between the geographic distribution of HLA-B27 alleles and their role in infectious and autoimmune diseases: a unifying hypothesis. *Autoimmun. Rev.* 8: 420–425.
59. Will, R., L. Edmunds, J. Elswood, and A. Calin. 1990. Is there sexual inequality in ankylosing spondylitis? A study of 498 women and 1202 men. *J. Rheumatol.* 17: 1649–1652.
60. Giltay, E. J., D. van Schaardenburg, L. J. Gooren, C. Popp-Snijders, and B. A. Dijkmans. 1999. Androgens and ankylosing spondylitis: a role in the pathogenesis? *Ann. N. Y. Acad. Sci.* 876: 340–364, discussion 365.
61. Lories, R. J., I. Derese, C. de Bari, and F. P. Luyten. 2007. Evidence for uncoupling of inflammation and joint remodeling in a mouse model of spondylarthritis. *Arthritis Rheum.* 56: 489–497.
62. van der Heijde, D., D. Salonen, B. N. Weissman, R. Landewé, W. P. Maksymowych, H. Kupper, S. Ballal, E. Gibson, and R. Wong, Canadian (M03-606) study group, ATLAS study group. 2009. Assessment of radiographic progression in the spines of patients with ankylosing spondylitis treated with adalimumab for up to 2 years. *Arthritis Res. Ther.* 11: R127.
63. Thomas, G. P., and M. A. Brown. 2010. Genetics and genomics of ankylosing spondylitis. *Immunol. Rev.* 233: 162–180.
64. Limón-Camacho, L., M. I. Vargas-Rojas, J. Vázquez-Mellado, J. Casasola-Vargas, J. F. Moctezuma, R. Burgos-Vargas, and L. Llorente. 2012. In vivo peripheral blood proinflammatory T cells in patients with ankylosing spondylitis. *J. Rheumatol.* 39: 830–835.
65. Abe, Y., M. Ohtsuji, N. Ohtsuji, Q. Lin, H. Tsurui, S. Nakae, T. Shirai, K. Sudo, and S. Hirose. 2009. Ankylosing enthesitis associated with up-regulated IFN-γ and IL-17 production in (BXSB × NZB) F_1 male mice: a new mouse model. *Mod. Rheumatol.* 19: 316–322.